Supplementary information

High Emission Quantum Yields and Color-Tunable Properties of Ln-Chelates Embedded in PMMA

Aneta Lipa,[a] Yen Hoang Pham,[a] Albano N. Carneiro Neto,*[b] Viktor A. Trush,[c] Huanrong Li,[d] Oscar L. Malta,[e] Volodymyr M. Amirkhanov,[c] and Paula Gawryszewska*[a]

[a] Faculty of Chemistry, University of Wroclaw, 14 F. Joliot-Curie Str., 50-383 Wroclaw, Poland
[b] Physics Department and CICECO-Aveiro Institute of Materials, University of Aveiro, Campus Universitário de Santiago, 3810-193 Aveiro, Portugal
[c] Department of Chemistry, Kyiv National Taras Shevchenko University, Volodymyrska str. 64, Kyiv 01601, Ukraine
[d] School of Chemical Engineering and Technology, Hebei University of Technology, Tianjin 300130, China
[e] Departamento de Química Fundamental, Universidade Federal de Pernambuco, Cidade Universitária, 50740-560 Recife, Brazil

e-mail: albanoneto@ua.pt and paula.gawryszewska-wilczynska@uwr.edu.pl

Abstract: This research presents a series of PMMA thin layers (labelled **Ln_PMMA**, where Ln = Eu^{3+}, Tb^{3+}, Sm^{3+}, Dy^{3+}) with high overall emission quantum yields of Q_{Eu}^{L} = 85%, Q_{Tb}^{L} = 66%, Q_{Sm}^{L} = 3 %, Q_{Dy}^{L} = 6 % with introduced lanthanide (Ln^{3+}) coordination compounds of the type $[Na_2LnL_4(OTf)(DMF)]$ (where L - N-(diphenylphosphoryl)-pyrazine-2-carboxamide, OTf = $[CF_3SO_3]^-$, DMF = N,N-dimethylformamide). This is the first analysis comparing the photophysical properties of coordination compounds encapsulated in PMMA with single crystals, which includes the influence of such factors as the inhomogeneity of the Ln^{3+} coordination polyhedra and the refractive index. A model is proposed to estimate the change in Q_{Ln}^{L} when the Ln chelat is incorporated into a PMMA medium, and it satisfactorily reproduces the experimental data with a maximum absolute error of 3% for the case of Eu^{3+} sample. At the same time, our work shows the influence of the PMMA matrix on the photophysical properties of Ln^{3+} with large (Eu, Tb) and small energy gap (Sm, Dy) between the emitting levels and adjacent levels with lower energy. Q_{Ln}^{L} for coordination compounds introduced into PMMA decreases relative to single crystals by about 10 % for Eu^{3+}, Tb^{3+} as well as by about 70 % for Sm^{3+} and Dy^{3+} for which emitting levels are quenched by the electron-phonon coupling presented by the vibrational modes of the PMMA matrix. **Ln_PMMA** thin layers containing a mixture of Eu^{3+}, Tb^{3+}, Sm^{3+} and Dy^{3+} coordination compounds are characterized by multicolor tunable emission.

DOI: 10.1039/D4TC03939D

Supplementary information

TABLE OF CONTENTS

Supplementary information

1. Spectroscopic characterization

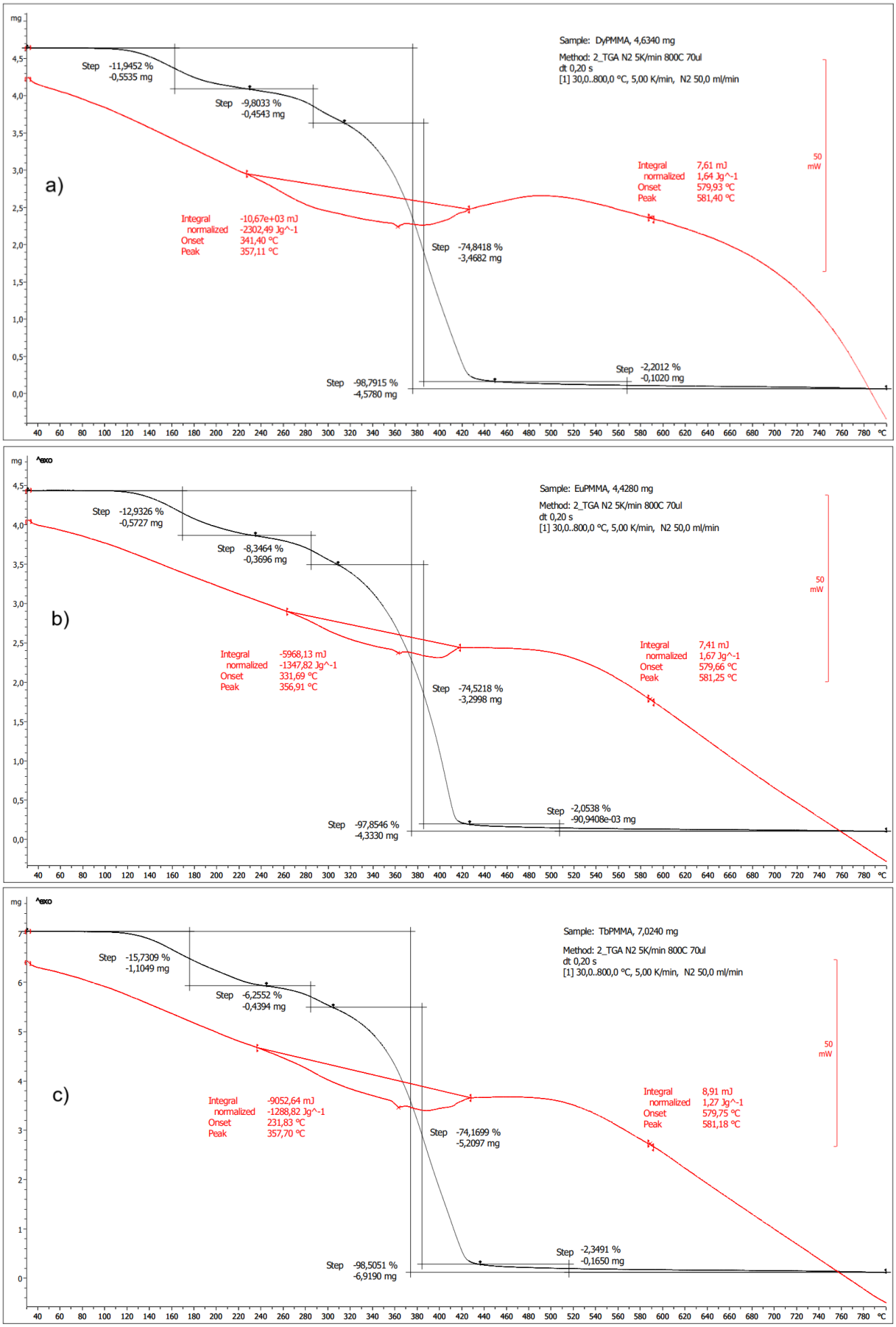

Supplementary information

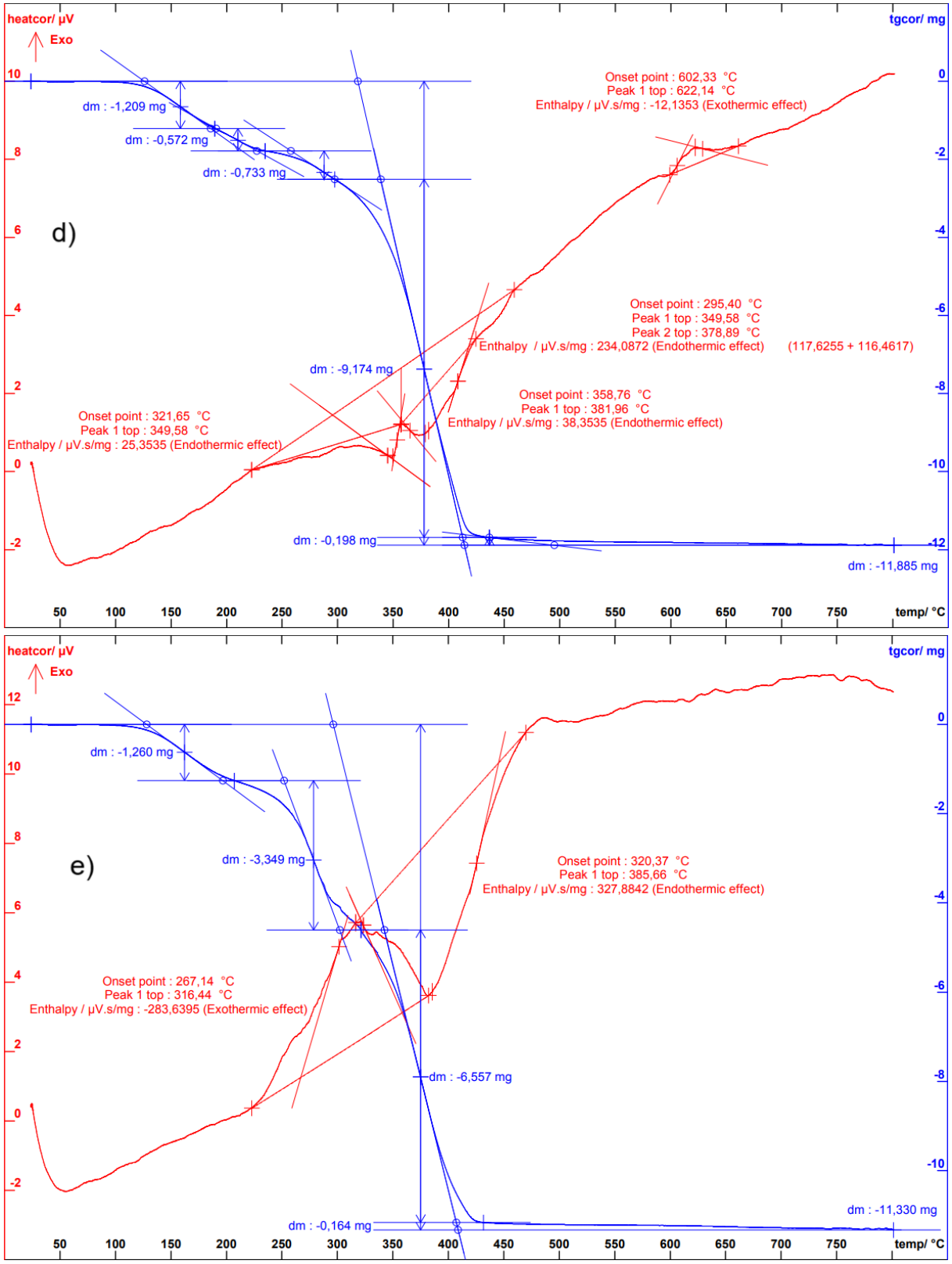

Figure S1. TGA thermograms of a) Dy_PMMA, b) Eu_PMMA, c) Tb_PMMA, d) Sm_PMMA, and e) PMMA under nitrogen atmosphere.

Supplementary information

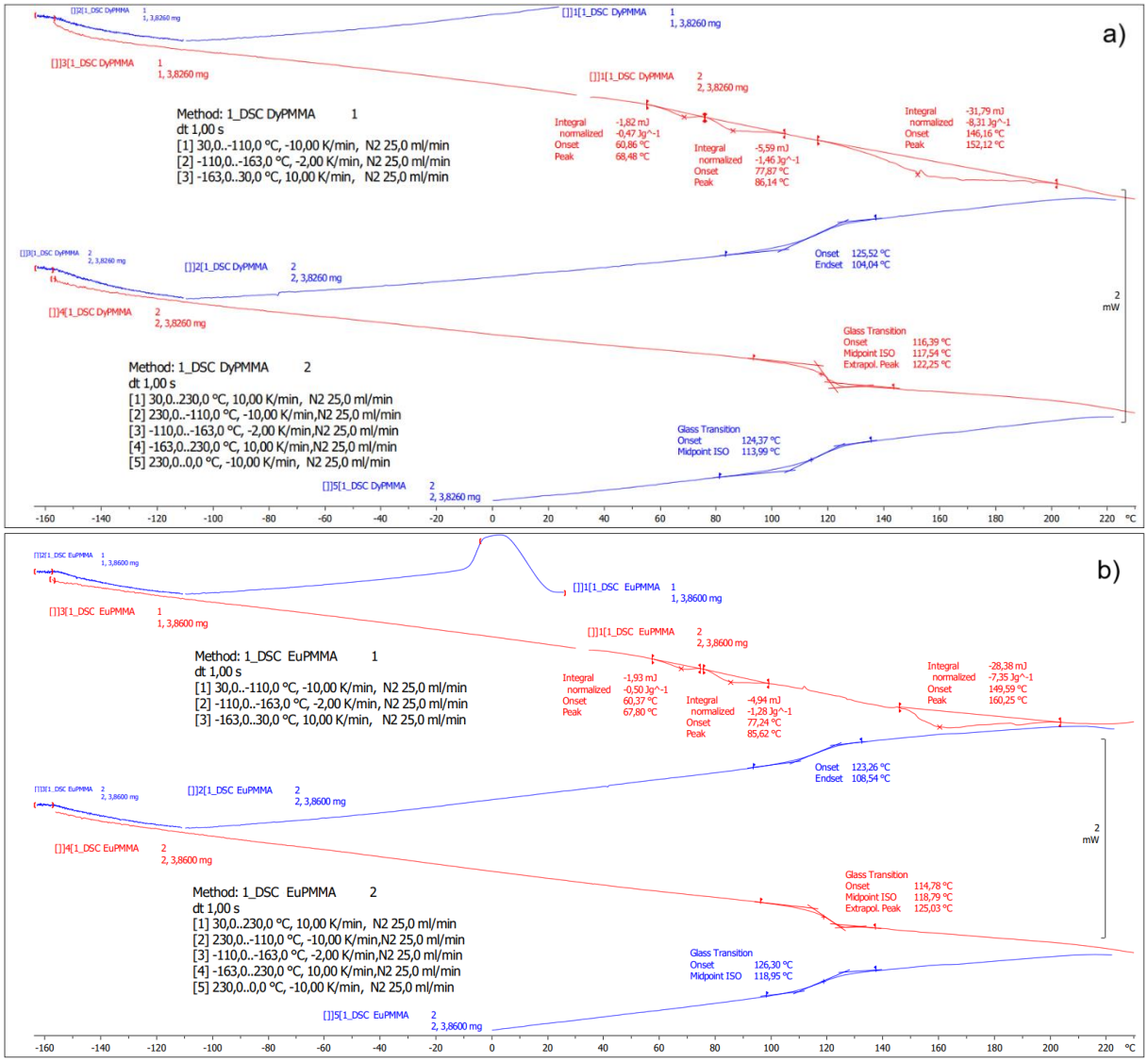

Supplementary information

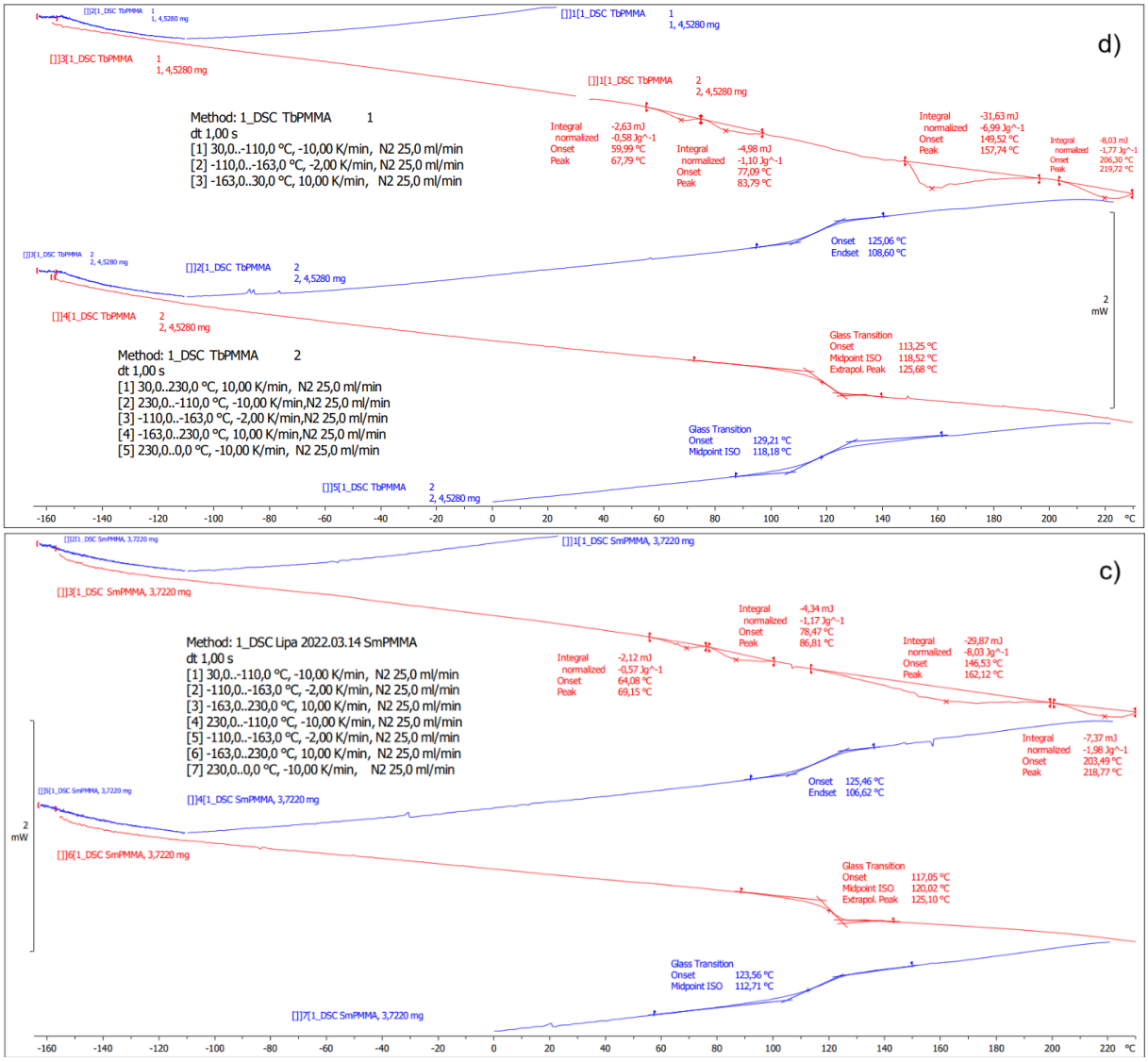

Figure S2. DSC curves of a) Dy_PMMA, b) Eu_PMMA, c) Sm_PMMA, and d) Tb_PMMA

Supplementary information

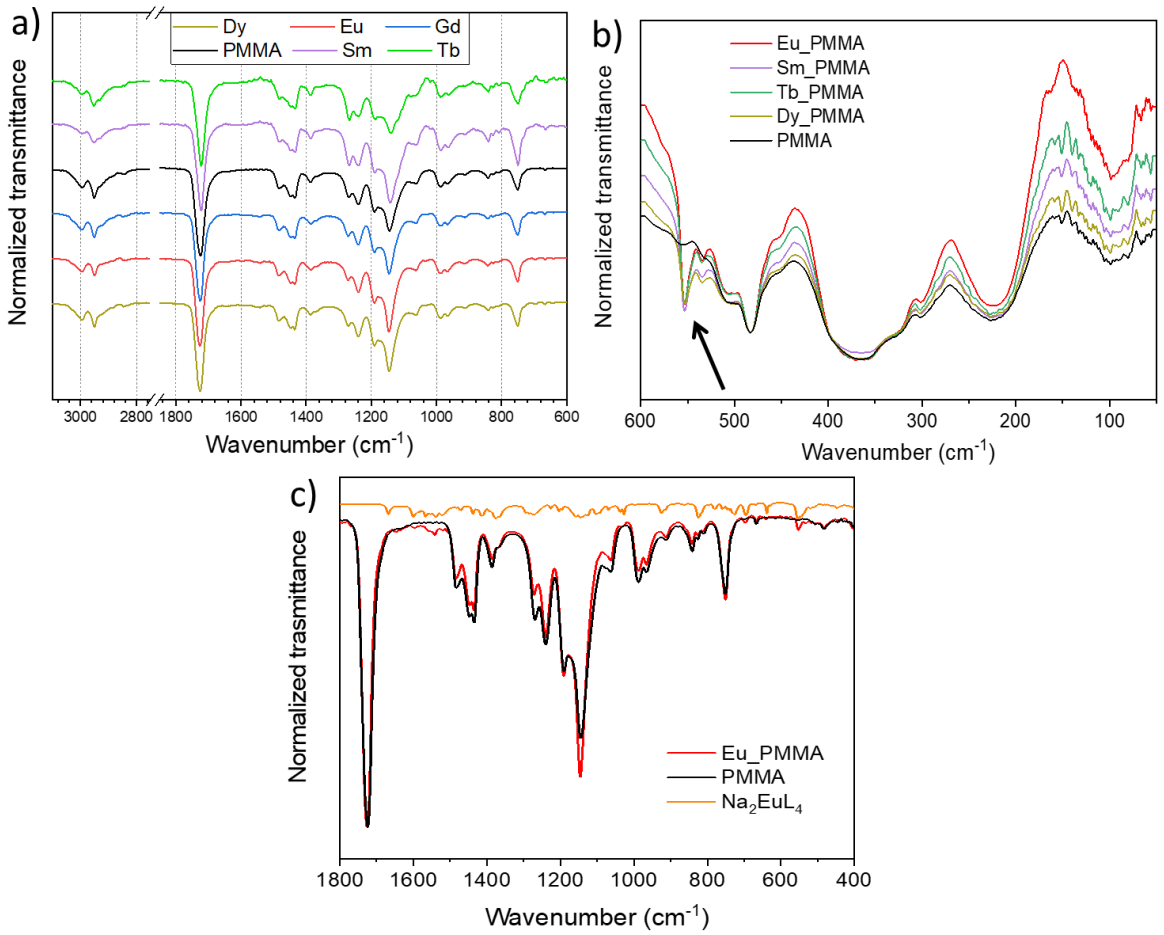

Figure S3. IR spectra of **Ln_PMMA** *(*a) in far IR region *(*b), c) **Eu_PMMA** in comparison with **PMMA** and **Na_2EuL_4**.

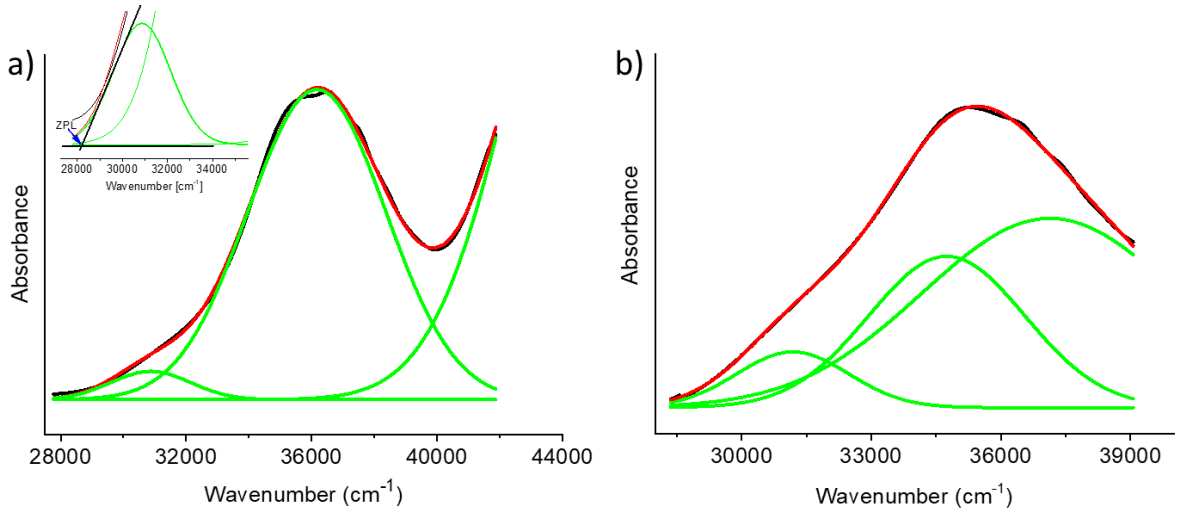

Figure S4. Absorption spectra of a) **Eu_PMMA** (black line) with Gaussian fitting curves (green line)at 295 K; the red line is the profile of the absorption spectrum obtained from Gaussian fitting (R^2 = 0.9990); b) **Na_2EuL_4** in the form of pellet mixed with KBr (black line) with Gaussian fitting curves (green line)at 295 K; the red line is the profile of the absorption spectrum obtained from Gaussian fitting (R^2 = 0.9998).

Supplementary information

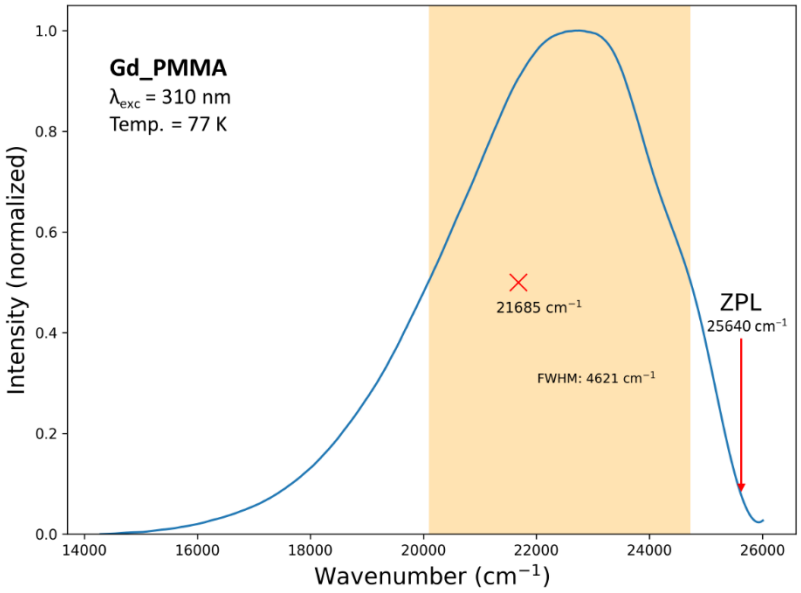

Figure S5. Phosphorescence spectrum of **Gd_PMMA** (λ_{exc} = 310 nm) at 77 K. The zero-phonon energy (ZPL, red arrow), barycenter (red cross) and the full width at half maximum (FWHM, the orange track centered at the barycenter) are indicated.

Emission spectra seen in Figures 3 and 4 were recorded for a PMMA layer of 2 wt. % coordination compounds. This value was chosen based on measurements of excitation spectra for **Eu_PMMA** with different contents of the **Na_2EuL_4** compound from 1 to 15 wt. %. Figure 5 shows a comparison of the excitation spectra of single crystals and PMMA thin layers with different chelate contents.

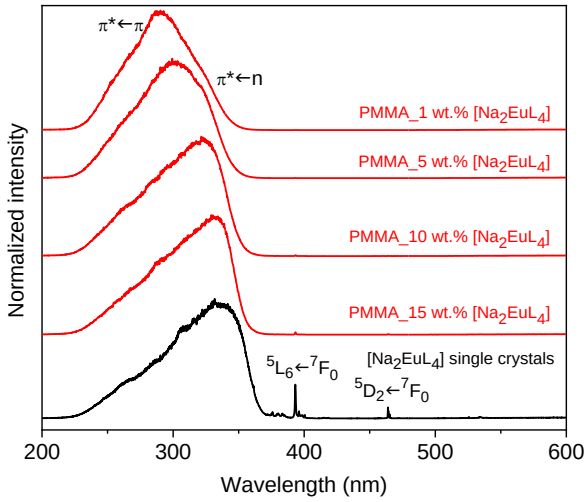

Figure S6. Excitation spectra of **Eu_PMMA** thin layers and **Na_2EuL_4** single crystals at 295 K.

It can be seen that the shape and spectral range of the band corresponding to the ligand absorption of **Na_2EuL_4** single crystals and **Eu_PMMA** with 15 wt. % chelate are the same. For **Eu_PMMA** (15 wt. %), a slight shift of the band maximum (by 2 nm) towards higher energies is observed. This shift increases with dilution and for 1 wt. % **Na_2EuL_4** equals 45 nm. The spectral range of the band also changes from 220- 372 nm for single crystals to 220-355 nm for **Eu_PMMA** with 1 wt. %. This behavior is due to the so-called surface quenching caused by strong absorption of radiation with a wavelength corresponding to the absorption maximum of the ligand. In order to obtain thin layers with minimized surface quenching effects, all investigations were carried out for PMMA with 2 wt. % chelates.

Supplementary information

Table S1. Emission decay times and overall emission quantum yield (Q_{Ln}^{L}).

Compounds	τ_{295K} (μs)/ λ_{exc} (nm)	τ_{77K} (μs)/ λ_{exc} (nm)	τ_{295K} (μs)/ λ_{exc} (nm)*	τ_{77K} (μs)/ λ_{exc} (nm)*	Q_{Ln}^{L} (%)
Na_2EuL_4 in PMMA	1776±4/320	1838±4/320	1758±4/464	1801±4/464	85 ± 8
Na_2EuL_4 crystals	1700±3/330	1710±3/330	there is no dependence of τ on λ_{exc}	there is no dependence of τ on λ_{exc}	95 ± 9
Na_2TbL_4 in PMMA	1780±2/320	1779±5/320	1739±5/478		66 ± 7
Na_2TbL_4 crystals	1604±3/330	1605±3/330	there is no dependence of τ on λ_{exc}	there is no dependence of τ on λ_{exc}	75 ± 8 value after time 2 years
Na_2SmL_4 in PMMA	159±1/320 81% 64±3/320 19%	175±1/320 87% 70±3/320 13%	146±1/402 88% 45±2/402 12%		3.0 ± 0.3
Na_2SmL_4 crystals	195±0.2/330	199 ±0.2/330	there is no dependence of τ on λ_{exc}	there is no dependence of τ on λ_{exc}	11 ± 1
Na_2DyL_4 in PMMA	106±2/320 78% 54±3/320 22%	118±2/320 82% 56±4/320 18%	97±1/386 94% 54±3/386 6%		6.0 ± 0.6
Na_2DyL_4 crystals	140±0.14/330	170±0.17/330	there is no dependence of τ on λ_{exc}	there is no dependence of τ on λ_{exc}	17 ± 2

Supplementary information

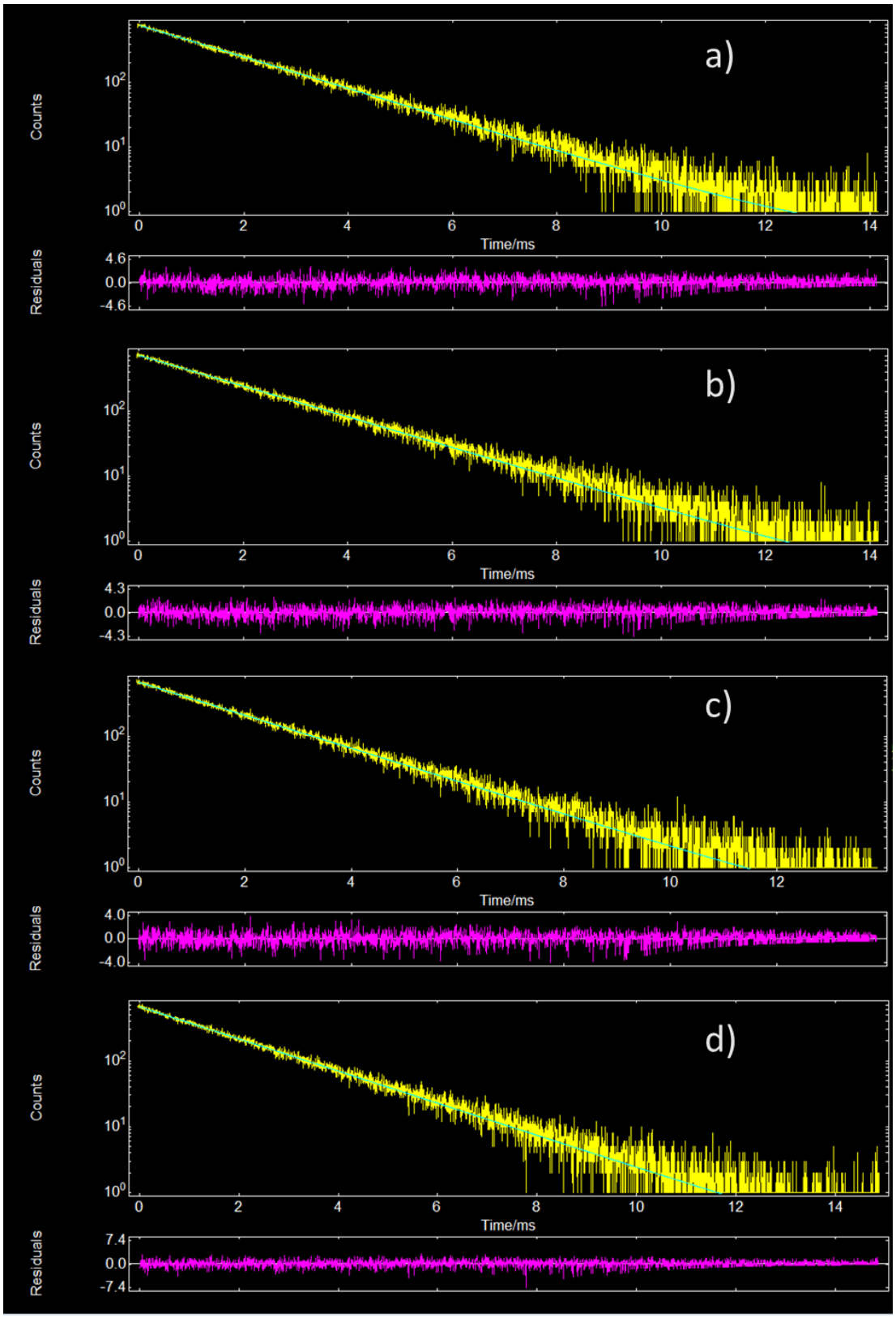

Figure S7. Luminescence decay time curves (yellow line), fit curves (green line) and fit regular residual plot (pink line).a) **Eu_PMMA**, λ_{exc} = 320 nm, λ_{mon} = 611.4 nm, χ^2 = 1.053 at 295 K; b) **Eu_PMMA**, λ_{exc} = 320 nm, λ_{mon} = 611.4 nm, χ^2 = 1.032 at 77 K; c) **Tb_PMMA**, λ_{exc} = 320 nm, λ_{mon} = 544.7 nm, χ^2 = 1.025 at 295 K; d) **Tb_PMMA**, λ_{exc} = 320 nm, λ_{mon} = 544.7 nm, χ^2 = 1.051 at 77 K. The same values of decay times were obtained when fitting with the OriginPro 8.6 program with R^2 = 0.996 for **Eu_PMMA** and 0.999 for **Tb_PMMA.**

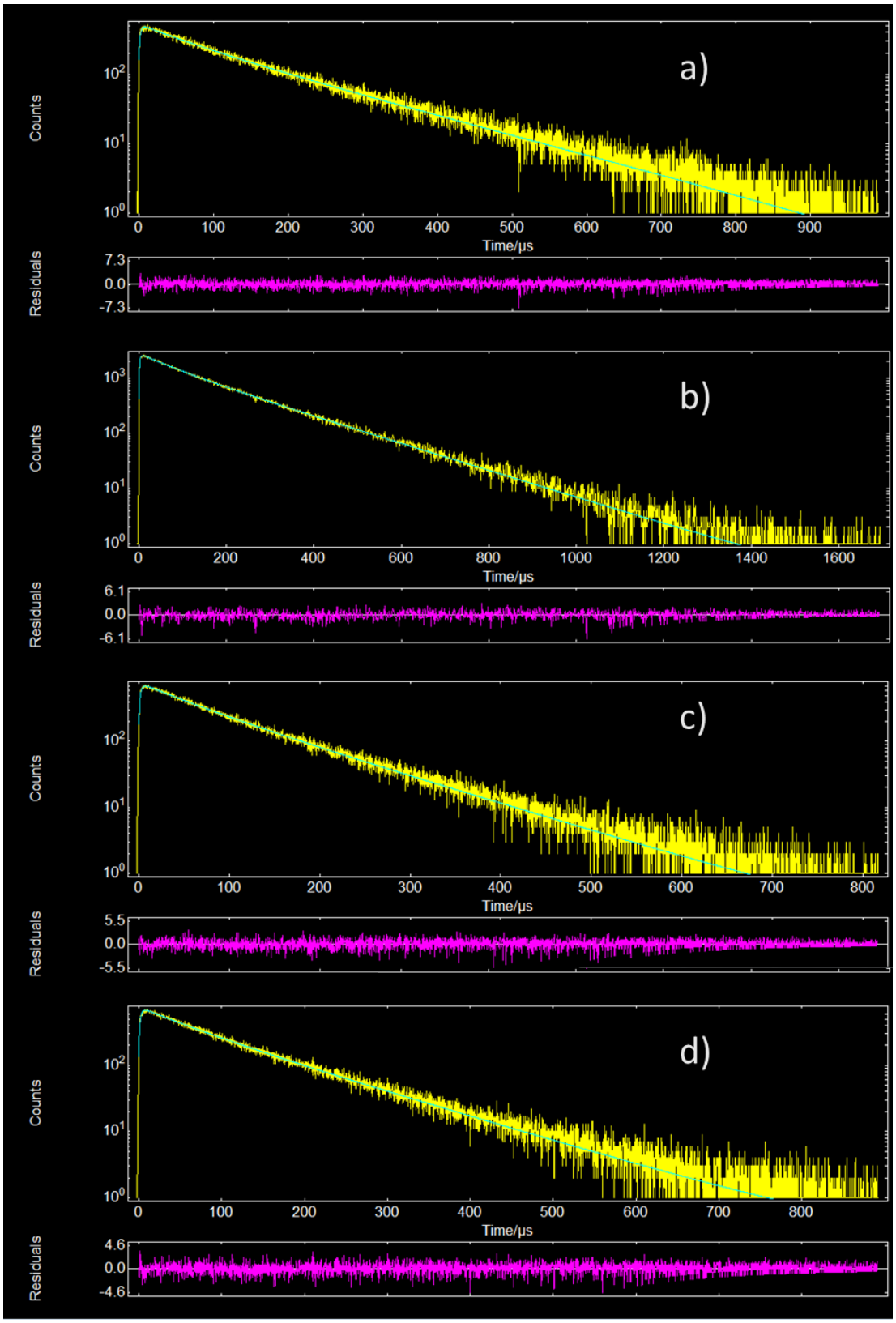

Figure S8. Luminescence decay time curves (yellow line), fit curves (green line) and fit regular residual plot (pink line). a) **Sm_PMMA**, λ_{exc} = 320 nm, λ_{mon} = 644.0 nm, χ^2 = 1.025 at 295 K; b) **Sm_PMMA**, λ_{exc} = 320 nm, λ_{mon} = 648.5 nm, χ^2 = 1.075 at 77 K; c) **Dy_PMMA**, λ_{exc} = 320 nm, λ_{mon} = 573.4 nm, χ^2 = 1.031 at 295 K; d) **Dy_PMMA**, λ_{exc} = 320 nm, λ_{mon} = 573.4 nm, χ^2 = 0.999 at 77 K.

Supplementary information

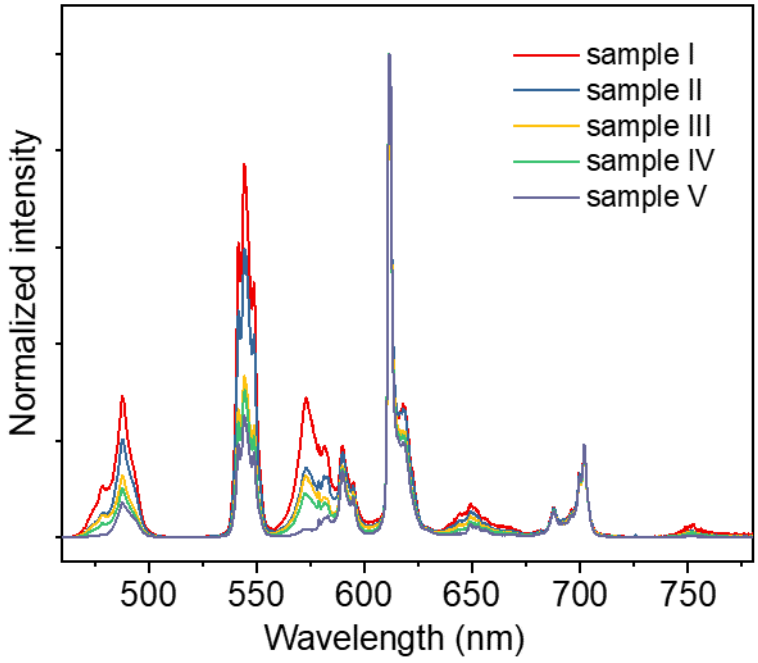

Figure S9. Emission spectra of five samples of mixed PMMA layers at 295 K, λ_{exc} = 320 nm.

2. Intensity parameters

2.1. Experimental intensity parameters

The 4*f*-4*f* transitions intensities in Eu^{3+}-based compounds can be expressed from the areas under their emission curves [1]. Thus, the experimental intensity parameters Ω_2, Ω_4 and Ω_6 can be estimated as follow,

$$\Omega_{\lambda}^{\exp} = \frac{3\hbar c^3 A_{0\to\lambda}}{4e^2\omega^3\chi\langle {}^7F_\lambda \| U^{(\lambda)} \| {}^5D_0\rangle^2} \quad \text{(S1)}$$

where $\chi = n(n^2+2)^2/9$ is the Lorentz local field correction and n is the linear index of refraction of the medium (n = 1.49 for **Ln_PMMA** and n = 1.61 for **Na_2LnL_4**). ω is the angular frequency of the transition, and $\boldsymbol{U}^{(\lambda)}$ are unity tensor operators. In the case of compounds containing the Eu^{3+} ion, the square of the reduced matrix elements $\langle {}^7F_\lambda \| U^{(\lambda)} \| {}^5D_0\rangle^2$ is numerically equal to 0.0032 and 0.0023 for λ = 2 and 4 [2], respectively. The spontaneous emission coefficients $A_{0\to J}$ can be estimated by:

$$A_{0\to J} = A_{0\to 1}\left(\frac{S_{0\to J}}{S_{0\to 1}}\right) \quad \text{(S2)}$$

$$A_{0\to 1} = \frac{e^2\omega^3\hbar}{3mc^5} n^3 \langle {}^7F_1 \| L + 2S \| {}^5D_0\rangle^2 \approx 14.65 \cdot n^3 \quad \text{(S3)}$$

The quantity $A_{0\to 1}$ can be used as an internal reference and corresponds to the spontaneous emission coefficient for the transition allowed by magnetic dipole $^5D_0 \to {}^7F_1$. The square of the reduced matrix element $\langle {}^7F_1 \| L + 2S \| {}^5D_0\rangle^2 = 0.116$ can be estimated using free-ion wavefunctions in the intermediate coupling scheme [3]. The values $S_{0\to J}$ are the integrated intensities (area under the emission curves) of $^5D_0 \to {}^7F_J$ (J = 0–6) and their observable values are listed in Table 2 ($^5D_0 \to {}^7F_5$ and $^5D_0 \to {}^7F_6$ emissions were not detected). In addition, once the $^5D_0 \to {}^7F_6$ transition was not observed, the experimental values of $\Omega_6^{\exp}$ will not be considered in this work. It is worth emphasizing that Eqs. S1–S3 are applicable only for Eu^{3+}-based compounds and, therefore, cannot be applied for any other lanthanide ions.

Supplementary information

2.2. Theoretical intensity parameters

In the absence of a center of inversion, the Forced Electric Dipole (FED – original Judd-Ofelt theory) and Dynamic Coupling (DC) mechanisms are responsible for the 4f-4f intensities. Thus, the theoretical intensity parameters $\Omega_\lambda^{\text{theo}}$ can be calculated by the following expressions,

$$\Omega_\lambda^{\text{theo}} = (2\lambda+1)\sum_{t,p}\frac{\left|B_{\lambda tp}\right|^2}{2t+1} \quad , \qquad B_{\lambda tp} = B_{\lambda tp}^{FED} + B_{\lambda tp}^{DC} \tag{S4}$$

where

$$B_{\lambda tp}^{FED} = \frac{2}{\Delta E}\langle r^{t+1}\rangle\Theta(t,\lambda)\left(\frac{4\pi}{2t+1}\right)^{\frac{1}{2}}\sum_j \frac{e^2\rho_j g_j\left(2\beta_j\right)^{t+1}}{R_j^{t+1}}\left(Y_p^{t*}\right)_j \tag{S5}$$

$$B_{\lambda tp}^{DC} = -\left[\frac{(\lambda+1)(2\lambda+3)}{(2\lambda+1)}\right]^{\frac{1}{2}}\langle r^\lambda\rangle\langle f\|C^{(\lambda)}\|f\rangle\left(\frac{4\pi}{2t+1}\right)^{\frac{1}{2}}\times\sum_j\frac{\left[\left(2\beta_j\right)^{t+1}\alpha_{OP,j}+\alpha_j'\right]}{R_j^{t+1}}\left(Y_p^{t*}\right)_j\delta_{t,\lambda+1} \tag{S6}$$

with *t* and *p* being the ranks and its components that define the conjugated complexes of the spherical harmonics $\left(Y_p^{t*}\right)$. The expressions in Eqs. S5 and S6 are derived from the Simple Overlap Model (SOM) [4,5] and Bond Overlap Model (BOM) [6,7], respectively. $\Theta(t,\lambda)$ are numerical factors which assume values of $\Theta(1,2)=-0.17, \Theta(3,2)=0.34, \Theta(3,4)=0.18; \Theta(5,4)=-0.24;\ \Theta(5,6)=-0.24$, and $\Theta(7,6)=0.24$ [8,9]. $\langle r^\lambda\rangle$ are 4f radial integrals and $\langle f\|C^{(\lambda)}\|f\rangle$ is equal to −1.366, 1.128, and −1.270 for λ = 2, 4, and 6, respectively. The overlap polarizabilities α_{OP} are quantities related to the degree of covalency of a chemical bond [6,10,11]. ρ is the overlap integral between 4f electrons of the lanthanide ion and the valence electrons of the ligating atom while $\beta=(1+\rho)^{-1}$. R is the Ln–ligating atom bond distance, e is the elementary charge of an electron, and $\delta_{t,\lambda+1}$ is a delta of Kronecker, which allows only the t = 3, 5, and 7 for λ = 2, 4, and 6, respectively.

With the structure and the experimental values of Ω_λ, the α' as well as the g values where extracted from a fitting procedure in the JOYSpectra program [12]. It is important to comment that the Ω_λ does not depend on the index of refraction (n) of the medium. However, the spontaneous emission coefficients have this dependence (Eq. S9).

Table S2. Theoretical intensity parameters calculated for the crystallographic structure (Ω_2, Ω_4, and Ω_6 in units of 10^{-20} cm^2), with no distortion (L = 0), and the average values $\bar{\Omega}_2$, $\bar{\Omega}_4$, and $\bar{\Omega}_6$ (in units of 10^{-20} cm^2) with maximum displacement L (in units of Å), for structures in PMMA. The experimental Ω_2^{exp} and Ω_4^{exp} values (in units of 10^{-20} cm^2) for the Eu^{3+} in **Na_2EuL_4** crystal and **Eu_PMMA** are displayed in parentheses.

	Ln^{3+}	Temp. (K)	$\boldsymbol{\Omega_2}$	$\boldsymbol{\Omega_4}$	$\boldsymbol{\Omega_6}$	L
Crystal	Eu^{3+}	77	8.2 (8.2)	4.7 (4.4)	0.7	0
	Eu^{3+}	300	9.3 (8.8)	4.8 (4.5)	0.8	0
	Tb^{3+}	77	6.6	3.6	0.5	0
	Tb^{3+}	300	7.5	3.7	0.5	0
	Sm^{3+}	77	9.3	6.3	1.1	0
	Sm^{3+}	300	10.6	6.4	1.1	0
	Dy^{3+}	77	6.2	4.6	0.5	0
	Dy^{3+}	300	7.0	4.7	0.5	0
	Ln^{3+}	Temp. (K)	$\boldsymbol{\bar{\Omega}_2}$	$\boldsymbol{\bar{\Omega}_4}$	$\boldsymbol{\bar{\Omega}_6}$	L
PMMA	Eu^{3+}	77	8.6 (10.0)	4.8 (6.3)	0.8	0.152
	Eu^{3+}	300	10.2 (10.3)	5.0 (6.3)	1.0	0.223
	Tb^{3+}	77	7.0	3.7	0.5	0.151
	Tb^{3+}	300	8.3	3.9	0.6	0.222
	Sm^{3+}	77	9.7	6.4	1.2	0.152
	Sm^{3+}	300	11.6	6.7	1.5	0.223
	Dy^{3+}	77	6.6	4.7	0.6	0.151
	Dy^{3+}	300	7.9	4.9	0.7	0.222

3. Theoretical emission quantum yield estimates

By its definition, the emission quantum yield is the ratio between emitted and absorbed photons. Therefore, it can be calculated as:

$$Q_{Ln}^{L} = \frac{\#emitted\ photons}{\#absorbed\ photons} = \frac{A_{rad} \cdot \eta_E}{\phi \cdot \eta_G} \tag{S7}$$

where A_{rad} (Eq. 3) is the total radiative rate (spontaneous emission coefficients), ϕ is the absorption pumping rate, η_E and η_G are the relative populations in the steady-state regime of the emitting and ground level, respectively. In such
Since the η_{sens} is not affected, we can confirm that the dynamics of intramolecular energy transfer (ligand-to-metal energy transfer) of **Na_2LnL_4** remains the same when it is incorporated into the PMMA matrix. Therefore, the populations remain the same, except for the cases of **Sm_PMMA** and **Dy_PMMA**, where their emitting levels are quenched by the electron-phonon coupling presented by the vibrational modes of the PMMA matrix. Consequently, the ratio $\eta_E/(\phi \cdot \eta_G)$ in Eq. S7 remains unchanged for Eu^{3+} and Tb^{3+} compounds. Under these conditions, we can propose the identity:

$$\frac{Q_{Ln}^{L}(P)}{A_{rad}(P)} = \frac{Q_{Ln}^{L}(C)}{A_{rad}(C)} \tag{S8}$$

where C and P represents the quantities (radiative rate and emission quantum yield) of the **Na_2LnL_4** in the crystal and PMMA, respectively. The general equation of the Einstein's spontaneous emission coefficient for a $|J'\rangle \rightarrow |J\rangle$ transition (for all lanthanide ions) is given by:

$$A_{rad}^{a\rightarrow b} = \frac{32\pi^3\left(\sigma_{J'\rightarrow J}\right)^3}{3\hbar(2G+1)}\left[\frac{n(n^2+2)^2}{9}S_{ed}^{J'\rightarrow J} + n^3 S_{md}^{J'\rightarrow J}\right] \tag{S9}$$

where $\hbar$ is the reduced Planck's constant, G is the emitting level degeneracy $|J'\rangle$, $\sigma_{J'\rightarrow J}$ is the wavenumber of the $|J'\rangle \rightarrow |J\rangle$ transition (in cm^{-1}), and n is the index of refraction of the medium. The quantities $S_{ed}^{J'\rightarrow J}$ and $S_{md}^{J'\rightarrow J}$ are the electric and magnetic dipole strengths if the transition, respectively. These quantities can be estimated from Eqs. S10 and S11:

$$S_{ed}^{J'\rightarrow J} = e^2\left(\sum_{\lambda=2,4,6}\Omega_\lambda \left|\langle J'\|U^{(\lambda)}\|J\rangle\right|^2\right) \tag{S10}$$

$$S_{md}^{J'\rightarrow J} = (\mu_B)^2|\langle J'\|L+2S\|J\rangle|^2 \tag{S11}$$

where $\mu_B = e\hbar/(2m_e c)$ is the Bohr magneton (m_e is the electron mass and c the speed of light), The values of matrix elements $\left|\langle J'\|U^{(\lambda)}\|J\rangle\right|^2$ and $|\langle J'\|L+2S\|J\rangle|^2$ are tabulated in references [2] and [9], respectively.

The magnetic dipole strength (Eq. S11) does not depend on the structure of the coordination polyhedron, while the electric dipole strength (Eq. S10) depends on the intensity parameters. Henceforth, we can overlook the contributions of magnetic dipole, as they are weaker than the electric dipole for Eu^{3+} and Tb^{3+} transitions. Therefore, we can develop Eq. S8 as:

$$\begin{aligned} Q_{Ln}^{L}(P) = Q_{Ln}^{L}(C)\frac{A_{rad}(P)}{A_{rad}(C)} &\approx Q_{Ln}^{L}(C)\frac{\sum_J \frac{32\pi^3\left(\sigma_{J'\rightarrow J}\right)^3}{3\hbar(2G+1)}\left[\frac{n_P({n_P}^2+2)^2}{9}S_{ed}^{J'\rightarrow J}(P)\right]}{\sum_J \frac{32\pi^3\left(\sigma_{J'\rightarrow J}\right)^3}{3\hbar(2G+1)}\left[\frac{n_C({n_C}^2+2)^2}{9}S_{ed}^{J'\rightarrow J}(C)\right]} \\ &= Q_{Ln}^{L}(C)\frac{\sum_J\left[\frac{n_P({n_P}^2+2)^2}{9}S_{ed}^{J'\rightarrow J}(P)\right]}{\sum_J\left[\frac{n_C({n_C}^2+2)^2}{9}S_{ed}^{J'\rightarrow J}(C)\right]} \\ &= Q_{Ln}^{L}(C)\frac{n_P({n_P}^2+2)^2\sum_J\left(\sum_\lambda \Omega_\lambda(P)\left|\langle J'\|U^{(\lambda)}\|J\rangle\right|^2\right)}{n_C({n_C}^2+2)^2\sum_J(\sum_\lambda \Omega_\lambda(C)\,|\langle J'\|U^{(\lambda)}\|J\rangle|^2)} \end{aligned} \tag{S12}$$

The separation of the sums in J and λ can be demonstrated:

Supplementary information

$$\sum_J \sum_\lambda \Omega_\lambda \left|\langle J'\|U^{(\lambda)}\|J\rangle\right|^2 = \sum_J \left(\Omega_2\left|\langle J'\|U^{(2)}\|J\rangle\right|^2 + \Omega_4\left|\langle J'\|U^{(4)}\|J\rangle\right|^2 + \Omega_6\left|\langle J'\|U^{(6)}\|J\rangle\right|^2\right) \tag{S13}$$

By developing the sum up J-terms from 1 to n elements:

$$\begin{aligned}\sum_{J=1}^{n} \left(\Omega_2\left|\langle J'\|U^{(2)}\|J\rangle\right|^2 + \Omega_4\left|\langle J'\|U^{(4)}\|J\rangle\right|^2 + \Omega_6\left|\langle J'\|U^{(6)}\|J\rangle\right|^2\right) \\ = \Omega_2\left|\langle J'\|U^{(2)}\|1\rangle\right|^2 + \Omega_2\left|\langle J'\|U^{(2)}\|2\rangle\right|^2 + \cdots + \Omega_2\left|\langle J'\|U^{(2)}\|n\rangle\right|^2 \\ + \Omega_4\left|\langle J'\|U^{(4)}\|1\rangle\right|^2 + \Omega_4\left|\langle J'\|U^{(4)}\|2\rangle\right|^2 + \cdots + \Omega_4\left|\langle J'\|U^{(4)}\|n\rangle\right|^2 \\ + \Omega_6\left|\langle J'\|U^{(6)}\|1\rangle\right|^2 + \Omega_6\left|\langle J'\|U^{(6)}\|2\rangle\right|^2 + \cdots + \Omega_6\left|\langle J'\|U^{(6)}\|n\rangle\right|^2\end{aligned} \tag{S14}$$

Note that we can rewrite the right-hand side of Eq. S14 as:

$$\Omega_2 \sum_J \left|\langle J'\|U^{(2)}\|J\rangle\right|^2 + \Omega_4 \sum_J \left|\langle J'\|U^{(4)}\|J\rangle\right|^2 + \Omega_6 \sum_J \left|\langle J'\|U^{(6)}\|J\rangle\right|^2 = \sum_\lambda \Omega_\lambda \sum_J \left|\langle J'\|U^{(\lambda)}\|J\rangle\right|^2 \tag{S15}$$

Substituting this relation in Eq. S12 we obtain:

$$Q^L_{Ln}(P) \approx Q^L_{Ln}(C)\frac{n_P({n_P}^2+2)^2\sum_\lambda \Omega_\lambda(P)\sum_J\left|\langle J'\|U^{(\lambda)}\|J\rangle\right|^2}{n_C({n_C}^2+2)^2\sum_\lambda \Omega_\lambda(C)\sum_J\left|\langle J'\|U^{(\lambda)}\|J\rangle\right|^2} = Q^L_{Ln}(C)\left(\frac{n_P({n_P}^2+2)^2}{n_C({n_C}^2+2)^2}\right)\underbrace{\left(\frac{\sum_\lambda \Omega_\lambda(P)}{\sum_\lambda \Omega_\lambda(C)}\right)}_{\Lambda} \tag{S16}$$

which assumes the form of Eq. 9.

The value of $\Lambda \approx 1.1$ can be computed from the calculated intensity parameters values at 300 K (Table S2):

$$\Lambda = \frac{\sum_\lambda \Omega_\lambda(P)}{\sum_\lambda \Omega_\lambda(C)} = \frac{\bar{\Omega}_2 + \bar{\Omega}_4 + \bar{\Omega}_6}{\Omega_2 + \Omega_4 + \Omega_6} = \frac{(10.2 + 5.0 + 1.0)\times 10^{-20}\ cm^2}{(9.3 + 4.8 + 0.8)\times 10^{-20}\ cm^2} \approx 1.09 \tag{S17}$$

Ln^{3+}

Eu^{3+}

$$\Lambda = \frac{(8.3 + 3.9 + 0.6)\times 10^{-20}\ cm^2}{(7.5 + 3.7 + 0.5)\times 10^{-20}\ cm^2} \approx 1.09 \tag{S18}$$

Tb^{3+}

$$\Lambda = \frac{(11.6 + 6.7 + 1.5)\times 10^{-20}\ cm^2}{(10.6 + 6.4 + 1.1)\times 10^{-20}\ cm^2} \approx 1.09 \tag{S19}$$

Sm^{3+}

$$\Lambda = \frac{(7.9 + 4.9 + 0.7)\times 10^{-20}\ cm^2}{(7.0 + 4.7 + 0.5)\times 10^{-20}\ cm^2} \approx 1.11 \tag{S20}$$

Dy^{3+}

4. Experimental emission quantum yield

Emission quantum yield is a very important parameter for assessing the suitability of a phosphor as well as comparing phosphors among themselves. One way to measure compounds in the solid state or thin layers is by integrating sphere. Contrary to appearances, this technique requires experience and care when measuring samples in the solid states, since the value of their quantum yield is affected by various factors that need to be known. An excellent source of information on this topic is the work on the first interlaboratory comparison of absolute emission quantum yield measurements to identify and quantify sources of uncertainty[13]. For our solid-phase compounds, **Na_2LnL_4**, the emission quantum yield (Q_{Ln}^L) was first reported in [14]. It was determined for a series of compounds (Ln = Eu, Tb, Sm, Dy) using an integrating sphere. A parallel control measurement was carried out for GOS:3%Eu and GOS:3%Tb compounds (GOS = Gd_2O_2S), for which the emission quantum yields are close to 100%. During the measurement for the empty sphere, a reference plug from Edinburg Instrument (Blanking Plug) was placed in the sample holder. During the measurements, no differences were observed for the sample in the form of very fine crystals (length on the order of tenths of a mm, and thickness on the order of hundredths of a mm), and the sample crushed in the mortar. In addition, Q_{Ln}^L was determined by the classical method developed at the Philips Research Laboratories[15] using an emission standard (GOS:3%Eu) and a scattering standard ($BaSO_4$). All compounds were ground so that the intensity of the non-absorbed radiation reflected by the sample surface and the two standards was identical (all experimental results are placed in ESI[14]). A result analogous to the technique using an integrating sphere was obtained.

For the purpose of this work, **Na_2EuL_4**, **Na_2SmL_4** and **Na_2DyL_4** compounds were obtained again (the old **Na_2TbL_4** was used from a desiccator), and their emission quantum yields were measured using an integrating sphere before introduction into PMMA. Information from the integrating sphere instructions recommends that *"For powder samples, a reference sample could be either a supplied reference plug (Blanking Plug) or $BaSO_4$ sample."*. In order to discern the effect of blank on the quantum yield value, parallel measurements were performed for GOS:3%Eu (from Phosphor Technology England) using the following holders when measuring the empty sphere: empty vessel, supplied reference plug (Blanking Plug), supplied reference plug (Blanking Plug) with lid, vessel with $BaSO_4$. Below is a table (Table S3) with one-time results trending repeatedly with subsequent measurements for GOS:Eu.

Table S3. Example one-time results of emission quantum yield values depending on the reference blanks used for empty integrating sphere measurements.

Blanks	**GOS:Eu**
empty vessel	1.13
supplied reference plug (Blanking Plug)	1.04
supplied reference plug+lid (Blanking Plug+lid)	1.22
vessel+$BaSO_4$	1.35
supplied reference plug after measurements	1.01

Based on the measurements performed with GOS:Eu powder, it was observed that:

- In case of our integrating sphere, emission quantum yield results are correct only when using the Blanking Plug (reference plug supplied);
- Sufficient sample should be used to cover the bottom of the holder; the presence of holder-bottom clearances generates a larger relative error (about 8% - five measurements); it makes no difference whether one uses a large amount of sample to fill the entire holder or enough to cover the entire bottom of the holder.
- The largest deviations in the value of emission quantum yield (overestimated values of more than 100%) are obtained for the vessel with $BaSO_4$. The average value of the positive relative error is 35% (five measurements). The trend is consistent with the results presented in[13].
- Grinding the sample in the case of very small crystals (our compound **Na_2LnL_4**) does not affect the Q_{Ln}^L result.

Given the tests performed, we believe it is good practice when measuring powders to check the quantum yields for solid emission standards.

For polymer thin layers, emission quantum yields were measured according to Edinburgh Instruments' recommendations that is, measurements were made for a sphere with a PMMA thin layer containing **Na_2LnL_4** compounds and for a sphere with a PMMA thin layer without **Na_2LnL_4**. In both cases, a single PMMA layer covered the surface of PTFE

trays. It turned out that for the layers with a thickness of 0.07 - 0.08 mm, whose edges were slightly raised at the edges due to their small thickness, the value of emission quantum yield was strongly dependent on the mutual position of the reference layers (without a lanthanide compound) and the measured ones (with the introduced **Na_2LnL_4**). The Q_{Eu}^L value also depends on the number of layers placed in PTFE trays. The value of Q_{Eu}^L in the cases mentioned above varied from about 60 to about 90%. Therefore, layers of greater thickness (0.17 – 0.21 mm) were obtained, which adhered to its surface and covered the surface of the PTFE trays during Q_{Ln}^L measurements. In this case, no effect of layer position on the Q_{Ln}^L value was observed.

Based on the above examples of Q_{Eu}^L measurements for PMMA layers, it should be emphasized that measuring emission quantum yield for polymer thin layers is not trivial and strongly depends on factors such as surface shape and number of polymer layers.

5. Refractive index

It should be remembered that the determined refractive indices are approximate values (average value due to biaxial crystals) and take on different values depending on the coordination compound of the lanthanide. Their value changes in a rather narrow range from values slightly lower than 1.5 [16] (n = 1.46) or slightly higher than 1.5 [17]. Moreover, lanthanide (Ln) coordination compounds often crystallize in the form of very small crystals, and often in triclinic, monoclinic or orthorhombic crystallographic systems (so-called biaxial crystals), which exhibit anisotropy of dielectric properties. This means that they have more than one refractive index. Thus, the value of 1.5 is assumed in the literature as the refractive index for Ln coordination compounds, and considering the difficulties in determining it, this is justified.

The refractive index measurements of **Na_2EuL_4** were performed as in ref. [17]. Measurements of the wavelength dependence of the refractive index in the range from 300 nm to 700 nm with a step of 100 nm were carried out using a transparent tablet made of ground single crystals (see Figure S11). At each wavelength, the measurement was performed in the angle range between 40 and 70 deg. Subsequently, each curve was adjusted (Fresnel's equation). The best fit was obtained in the 46 – 69 degree angle range. It should be noted that this is an average value, since the single crystals belong to a triclinic system, so they are not uniaxial, so they do not have a single refractive index.

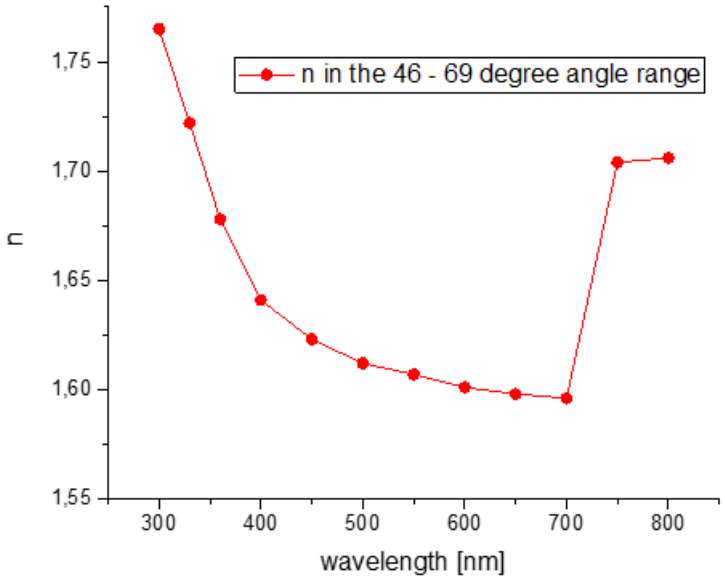

Figure S10. Dependence of the refractive index value of **Na_2EuL_4** on wavelength in the 46 – 69 degree angle range. In this case, the results for 750 and 800 nm should be rejected. Probably the light from the IR grating is not in the optical axis of the attachment.

Supplementary information

The measurement was repeated for a table prepared from uncrushed very small crystals. The tablet was less transparent and the surface was not smoothed. The results of the refractive index measurement are shown in Figure 11.

References

1 A. N. Carneiro Neto, E. E. S. Teotonio, G. F. de Sá, H. F. Brito, J. Legendziewicz, L. D. Carlos, M. C. F. C. Felinto, P. Gawryszewska, R. T. Moura, R. L. Longo, W. M. Faustino and O. L. Malta, in *Handbook on the Physics and Chemistry of Rare Earths*, eds. J.-C. G. Bünzli and V. K. Pecharsky, Elsevier, 2019, pp. 55–162.

2 W. T. Carnall, H. Crosswhite and H. M. Crosswhite, *Energy level structure and transition probabilities in the spectra of the trivalent lanthanides in LaF_3*, Argonne, IL, United States, 1978.

3 G. S. Ofelt, *J. Chem. Phys.*, 1963, **38**, 2171–2180.

4 O. L. Malta, *Chem. Phys. Lett.*, 1982, **87**, 27–29.

5 O. L. Malta, *Chem. Phys. Lett.*, 1982, **88**, 353–356.

6 R. T. Moura Jr., A. N. Carneiro Neto, R. L. Longo and O. L. Malta, *J. Lumin.*, 2016, **170**, 420–430.

7 A. N. Carneiro Neto, R. T. Moura, E. C. Aguiar, C. V Santos and M. A. F. L. B. de Medeiros, *J. Lumin.*, 2018, **201**, 451–459.

8 O. L. Malta, S. J. L. Ribeiro, M. Faucher and P. Porcher, *J. Phys. Chem. Solids*, 1991, **52**, 587–593.

9 V. Trannoy, A. N. Carneiro Neto, C. D. S. Brites, L. D. Carlos and H. Serier-Brault, *Adv. Opt. Mater.*, 2021, **9**, 2001938.

10 O. L. Malta, H. J. Batista and L. D. Carlos, *Chem. Phys.*, 2002, **282**, 21–30.

11 R. T. Moura Jr., G. C. S. Duarte, T. E. da Silva, O. L. Malta and R. L. Longo, *Phys. Chem. Chem. Phys.*, 2015, **17**, 7731–7742.

12 R. T. Moura Jr., A. N. Carneiro Neto, E. C. Aguiar, C. V. Santos-Jr., E. M. de Lima, W. M. Faustino, E. E. S. Teotonio, H. F. Brito, M. C. F. C. Felinto, R. A. S. Ferreira, L. D. Carlos, R. L. Longo and O. L. Malta, *Opt. Mater. X*, 2021, **11**, 100080.

13 S. Fiedler, F. Frenzel, C. Würth, I. Tavernaro, M. Grüne, S. Schweizer, A. Engel and U. Resch-Genger, *Anal. Chem.*, 2024, **96**, 6730–6737.

14 Y. H. Pham, V. A. Trush, A. N. Carneiro Neto, M. Korabik, J. Sokolnicki, M. Weselski, O. L. Malta, V. M. Amirkhanov and P. Gawryszewska, *J. Mater. Chem. C*, 2020, **8**, 9993–10009.

15 A. W. . de Jager-Veenis and A. Bril, *PHILIPS J. RES.*, 1978, **33**, 124–132.

16 E. Kasprzycka, A. N. Carneiro Neto, V. A. Trush, O. L. Malta, L. Jerzykiewicz, V. M. Amirkhanov, J. Legendziewicz and P. Gawryszewska, *Spectrochim. Acta Part A Mol. Biomol. Spectrosc.*, 2022, **274**, 121072.

17 E. Kasprzycka, V. A. Trush, V. M. Amirkhanov, L. Jerzykiewicz, O. L. Malta, J. Legendziewicz and P. Gawryszewska, *Chem. – A Eur. J.*, 2017, **23**, 1318–1330.